

Non-reciprocal frequency conversion and mode routing in a microresonator

Zhen Shen^{1,2,*}, Yan-Lei Zhang^{1,2,*}, Yuan Chen^{1,2}, Yun-Feng Xiao³,
Chang-Ling Zou^{1,2}, Guang-Can Guo^{1,2}, and Chun-Hua Dong^{1,2†}

¹CAS Key Laboratory of Quantum Information, University of Science and Technology of China, Hefei 230026, P. R. China.

²CAS Center For Excellence in Quantum Information and Quantum Physics,

University of Science and Technology of China, Hefei, Anhui 230026, P. R. China. and

³State Key Laboratory for Mesoscopic Physics and Frontiers Science Center for Nano-optoelectronics,
School of Physics, Peking University, Beijing 100871, China

(Dated: January 27, 2022)

The transportation of photons and phonons typically obeys the principle of reciprocity. Breaking reciprocity of these bosonic excitations will enable the corresponding non-reciprocal devices, such as isolators and circulators [1–3]. Here, we use two optical modes and two mechanical modes in a microresonator to form a four-mode plaquette via radiation pressure force. The phase-controlled non-reciprocal routing between any two modes with completely different frequencies is demonstrated, including the routing of phonon to phonon (MHz to MHz), photon to phonon (THz to MHz), and especially photon to photon with frequency difference of around 80 THz for the first time. In addition, one more mechanical mode is introduced to this plaquette to realize a phononic circulator in such single microresonator. The non-reciprocity is derived from interference between multi-mode transfer processes involving optomechanical interactions in an optomechanical resonator. It not only demonstrates the non-reciprocal routing of photons and phonons in a single resonator but also realizes the non-reciprocal frequency conversion for photons and circulation for phonons, laying a foundation for studying directional routing and thermal management in an optomechanical hybrid network.

Optical and acoustic non-reciprocal devices are the basic building blocks for information processing and sensing based on photons and phonons. For bosons, several methods can be used to achieve non-reciprocity, ranging from applying a magnetic field [2, 4], imposing rotational motion [5–8], optomechanical interactions [9–13], spatiotemporal modulations [14–20], and chiral interaction of atoms [21–23]. Magnetically induced non-reciprocity, as the most common mechanism, is challenging to integrate low-optical-loss magnetic materials on chip for optical devices [4] and typically produce mm-scale phononic devices because of weak non-reciprocal absorption [24, 25]. The optomechanical systems [26, 27], are one of the most promising candidates to realize magnetic-free non-reciprocity [28, 29], where the optical isolation and non-reciprocal control of phonons have been demonstrated respectively. Among them, one non-reciprocal mechanism is the use of phase matching conditions of traveling wave modes [28, 30–33]. Another mechanism is based on the gauge phase in the network of multiple nodes, which highlights the phase control of non-reciprocity [10–12, 34–36]. Similar mechanisms have been applied to microwave photons in superconducting circuits [37–42]. Although the non-reciprocal mode conversion in superconducting circuits is demonstrated over a few gigahertz, applying the gauge phase mechanism to frequency dimension of optical photons and more modes in optomechanical systems will provide more non-trivial devices, such as phase-controlled non-reciprocal frequency conversion and phononic circulator.

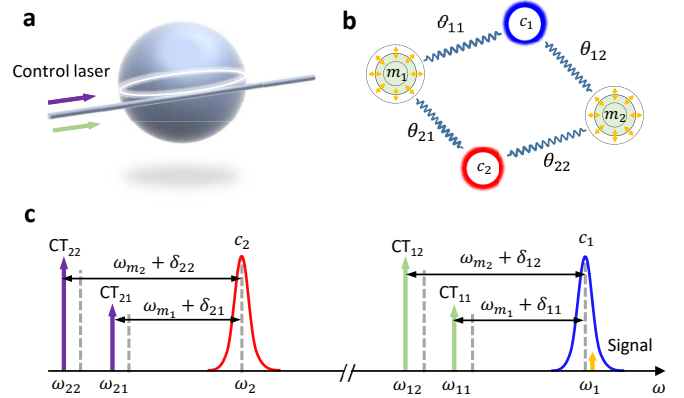


FIG. 1. **Schematic of the non-reciprocal routing in a microresonator.** **a.** The control lasers enhance the optomechanical coupling and control the non-reciprocal transportation inside a microsphere. **b-c.** The typical two optical modes with frequencies ω_1 and ω_2 and two mechanical modes with frequencies ω_{m_1} and ω_{m_2} are used to establish a four-mode plaquette via optomechanical interactions, which is controlled by four red-detuned control fields. The non-reciprocal effects can be changed by tuning the control phase θ_{11} , θ_{12} , θ_{21} and θ_{22} .

Here, we study the non-reciprocal routing of both photons and phonons in a microresonator, where two optical modes and two mechanical modes are exploited to form a closed loop of a four-mode plaquette, using the optomechanical interactions as shown in Figs. 1a-b. The four modes have completely different frequencies, i.e., 388

THz, 309 THz, 117 MHz, and 79 MHz, respectively. The non-reciprocal routing between any two nodes among these four modes is demonstrated, including the routing of phonon-phonon (MHz - MHz), photon-photon (THz - THz), and photon-phonon (THz - MHz). In general, the non-reciprocity results from the interference between two transportation paths engineered to connect the targeted nodes. The interference phase is governed by the phase of the control field, leading to a phase-controlled and flexible non-reciprocal routing. We demonstrate the phononic circulator simultaneously controlled by two independent phases when one more mechanical mode is introduced to such plaquette. The non-reciprocal frequency conversion opens new possibilities in communication and information processing, especially in the optical domain for wavelength-division-multiplexing (WDM) networks and quantum interface connecting separated systems operating at incompatible frequencies [43–45]. The phononic circulator holds great potential in thermal management, heat transfer, and phononics-based information processing [10].

Theoretical model

The hybrid plaquette includes two optical modes and two mechanical modes in the microresonator, as shown in Figs. 1b-c. The bosonic operators c_1 and c_2 denote two optical whispering-gallery modes with resonance frequencies of ω_1, ω_2 and dissipation rates of κ_1, κ_2 , respectively. The bosonic operators m_1 and m_2 denote two mechanical modes with resonance frequencies of $\omega_{m_1}, \omega_{m_2}$ and dissipation rates of γ_1, γ_2 . We focus on achieving non-reciprocal routing between any two nodes of these four modes, that is, the bosonic excitations in one mode can be unidirectionally converted to another mode. A total of six pairs transportation (m_1 - m_2 , c_1 - c_2 , c_j - m_k for $j, k \in \{1, 2\}$) should be respectively considered. Due to the symmetry, we select three pairs of nodes (m_1 - m_2 , c_1 - c_2 , c_1 - m_1) for experimental verification, showing that the non-reciprocal routing can be implemented between phonon-phonon, photon-photon, and photon-phonon in the plaquette, where the non-reciprocal mechanism can be fully described by the general theory of symmetry breaking between the two optomechanical coupling paths.

Here, we only theoretically describe the non-reciprocal routing of m_1 - m_2 in detail (other non-reciprocal routings are discussed in the Supplemental Material). When the cavity mode c_1 is driven by two optical tones with frequencies of ω_{11} and ω_{12} , the phonon of one mechanical mode up-converts to the optical mode c_1 and then down-converts to the other mechanical mode. As this process of frequency conversion features reciprocity, the cavity mode c_2 is introduced by the second pair of tones with frequencies of ω_{21} and ω_{22} , to form another path of

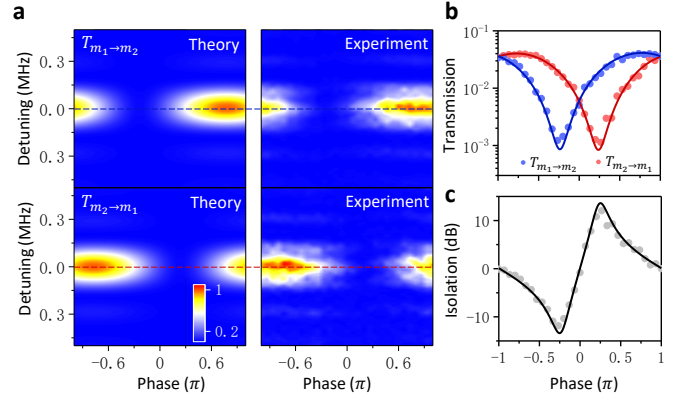


FIG. 2. **Non-reciprocal routing between the two mechanical modes.** **a.** Theoretical and experimental normalized power spectra $m_{2,out}$ ($m_{1,out}$) converted from $m_{1,in}$ ($m_{2,in}$) as the function of controlled phase θ . **b.** The transmissions $T_{m_1 \rightarrow m_2}$ and $T_{m_2 \rightarrow m_1}$ versus the control phase are obtained using the spectra data in **a** (the dashed blue line for $T_{m_1 \rightarrow m_2}$ and the dashed red line for $T_{m_2 \rightarrow m_1}$). **c.** The isolation $I = 10 \log(T_{m_1 \rightarrow m_2}/T_{m_2 \rightarrow m_1})$ as a function of the controlled phase, indicating more than 10 dB isolation in both directions in a reconfigurable manner. The solid lines in (b, c) indicate theoretically expected values.

optically mediated frequency conversion simultaneously. Based on the path interference, the hopping phases controlled through external drives in such a plaquette give rise to the non-reciprocal routing [37–39]. In the frame rotating at the frequencies ω_{jk} , the linearized Hamiltonian can be written as ($\hbar = 1$)

$$H = \sum_{j,k=1,2} G_{jk} \left[c_j^\dagger m_k e^{i(\delta_{jk}t + \theta_{jk})} + c_j m_k^\dagger e^{-i(\delta_{jk}t + \theta_{jk})} \right], \quad (1)$$

where the driving fields are around the red sideband of the cavity with the detuning $\delta_{jk} = \omega_j - \omega_{jk} - \omega_{m_k}$. And the counter-rotating terms can be neglected in the weak coupling regime $G_{jk} \ll \omega_{m_k}, |\omega_{m_2} - \omega_{m_1}|$. $G_{jk} = g_{jk} \sqrt{n_{jk}}$ is the effective optomechanical interaction strength with the vacuum optomechanical coupling rate g_{jk} and the total number of intracavity photons n_{jk} , and θ_{jk} is the relative phase set by driving fields.

For the interference of the two conversion paths, the effective phase $\delta_{jk}t + \theta_{jk}$ determines the non-reciprocity and conversion efficiency. For the non-reciprocal transportation between two mechanical modes, we set the cavity detunings $\delta_{11} = \delta_{12} = -\delta$ and $\delta_{21} = \delta_{22} = \delta$. And we define the transmission $T_{a \rightarrow b} = |b_{out}/a_{in}|^2$ with $a, b \in \{m_1, m_2, c_1, c_2\}$. The ratio η (See the Supplemental Material) of backward to forward transmission reads

$$\eta = \frac{T_{m_1 \rightarrow m_2}}{T_{m_2 \rightarrow m_1}} = \left| \frac{G_{11}G_{12}e^{-i\theta}\chi_1(\omega) + G_{21}G_{22}\chi_2(\omega)}{G_{11}G_{12}e^{i\theta}\chi_1(\omega) + G_{21}G_{22}\chi_2(\omega)} \right|^2, \quad (2)$$

where $\theta = \theta_{11} + \theta_{12} - \theta_{21} - \theta_{22}$. ω is the detuning between the signal and mode resonance, and $\chi_j^{-1} = \kappa_j/2 - i[\omega + (-1)^j \delta]$ is the optical susceptibility with $j \in \{1, 2\}$. Obviously, we have the ratio $\eta = 1$ when $\theta = n\pi$ with $n = 0, \pm 1, \pm 2, \dots$, which means that there is no non-reciprocity for any detuning δ and frequency ω . When the cooperativities for all four optomechanical couplings are equal ($C = C_{jk} = 4G_{jk}^2/\kappa_j\gamma_k$), we can obtain the perfect non-reciprocity, i.e. $\eta = 0$ or $\eta = \infty$, where the phase satisfies

$$\tan(\theta) = \pm \frac{\delta(\kappa_1 + \kappa_2) + \omega(\kappa_1 - \kappa_2)}{\kappa_1\kappa_2/2 - 2(\delta^2 - \omega^2)}. \quad (3)$$

In a practical experimental system, $\kappa_1 \neq \kappa_2$ and the non-reciprocity still exists when $\delta = 0$. However, we usually choose an appropriate δ in the experiment for an optimized non-reciprocity. In addition, due to the symmetry of four-mode plaquette, the cavity detunings should be changed as $\delta_{11} = \delta_{21} = -\delta$ and $\delta_{12} = \delta_{22} = \delta$ for the photon-photon non-reciprocity. For the adjacent conversion in such plaquette, i.e., phonon-photon conversion, the cavity detunings as mentioned before are all satisfied for the non-reciprocal routing (see Supplemental Material for more details).

Experimental realization

To experimentally demonstrate the non-reciprocal routing between any two nodes in the four-modes plaquette, a silica microsphere with a diameter of approximately $40 \mu\text{m}$ is used in our experiment, where we choose two whispering-galley modes with resonance frequency $\omega_1/2\pi = 387.56 \text{ THz}$ (near 774 nm), damping rates $\kappa_1/2\pi = 7 \text{ MHz}$ and $\omega_2/2\pi = 308.93 \text{ THz}$ (near 971 nm), $\kappa_2/2\pi = 27 \text{ MHz}$, respectively. The two radial breathing mechanical modes have frequencies of $\omega_{m_1}/2\pi = 79 \text{ MHz}$ and $\omega_{m_2}/2\pi = 117 \text{ MHz}$ with dissipation rates of $\gamma_1/2\pi = 9 \text{ kHz}$ and $\gamma_2/2\pi = 28 \text{ kHz}$, respectively (see Supplementary Material for more details regarding the setup).

Figure 2 shows the demonstrated experiment of non-reciprocal routing between the two mechanical modes, where the resonator is driven with four control fields (CT_{11} , CT_{12} , CT_{21} , CT_{22}) with powers (P_{11} , P_{12} , P_{21} , P_{22}) = (1.8, 3.5, 1.1, 4.5) mW that correspond to the cooperativities (C_{11} , C_{12} , C_{21} , C_{22}) = (3.6, 0.46, 0.73, 1). The control fields are locked at a frequency detuning from the lower motional sidebands of $\delta_{11}/2\pi = \delta_{12}/2\pi = -3 \text{ MHz}$ and $\delta_{21}/2\pi = \delta_{22}/2\pi = 3 \text{ MHz}$. Here, the control lasers are respectively modulated by the acoustic-optic modulators (AOMs) for pulse sequences to avoid thermal instability in the high-Q microresonator. And the four control tones are all phase-locked through the RF drives of AOMs, which can be varied continuously

from $-\pi$ to π . As a first step, the phonons $m_{1,in}$ (or $m_{2,in}$) are prepared from the converted optical signal, which is resonant on the mode c_1 and converted by a red-detuned control tone CT_{11} (or CT_{12}) served as writing pulse [43, 46, 47]. Then all control tones are turned on simultaneously for an interaction duration $\tau = 5 \mu\text{s}$ to transfer the excitations from mode m_1 (m_2) to m_2 (m_1). Finally, a control pulse CT_{12} (CT_{11}) served as a readout pulse interacts with the converted mechanical excitations, converting the mechanical excitations back to an optical pulse at the cavity resonance, which corresponds to the retrieval process of the optomechanical light storage [46, 47]. Figure 2a shows the normalized power spectra of the mode $m_{2,out}$ (or $m_{1,out}$) transferred from $m_{1,in}$ (or $m_{2,in}$). The non-overlap transmittance unambiguously present phase-controlled non-reciprocal routing: with $\theta = 0.27\pi$ the excitations prepared in mode m_1 is transferred to mode m_2 ($T_{m_1 \rightarrow m_2} \approx 1.8\%$) but not vice versa, while with $\theta = -0.27\pi$ the excitations prepared in mode m_2 is transferred to mode m_1 but not vice versa. The average phonon occupation $N_{m_{2,out}}$ (or $N_{m_{1,out}}$) is estimated through the spectrally integrated area of the displacement power density spectrum of the mechanical excitation. We have used the thermal displacement power density spectrum and the corresponding average thermal phonon number, $N_{m_{2,th}}$ (or $N_{m_{1,th}}$), to calibrate the measurement. The transmissions $T_{m_1 \rightarrow m_2}$ and $T_{m_2 \rightarrow m_1}$ are summarized and plotted in Fig. 2b as a function of the control phase θ (see Supplementary Material for more details with regard to the measurement). Therefore, isolation of more than 10 dB is demonstrated in each direction in a reconfigurable manner, that is, the direction of isolation can be switched by taking $\theta \rightarrow -\theta$, as shown in Fig. 2c.

Next, we experimentally realize the non-reciprocal routing of photons between the two optical modes c_1 and c_2 through two mechanical modes instead of the reciprocal photons conversion via one mechanical mode [30, 43]. At this point, the detunings of the four control tones are tuned to a new configuration ($\delta_{11}/2\pi = \delta_{21}/2\pi = -45 \text{ kHz}$, $\delta_{12}/2\pi = \delta_{22}/2\pi = 45 \text{ kHz}$) to establish the asymmetric paths achieving non-reciprocity. The pulse sequence and the phase of the control field are generated similarly with the case of non-reciprocal conversion of phonons (see Supplementary Material for more details). The signal photons injected on resonance with one optical mode will be converted to the other one, while four control fields are synchronously to drive the mechanical motions. Frequency conversion in both directions, $T_{c_1 \rightarrow c_2}$ and $T_{c_2 \rightarrow c_1}$ are measured and compared for three different phases in Fig. 3a. At $\theta = 0.73\pi$, we observe relatively high forward transmittance (6%) from cavity 1 to 2 and near-zero transmittance (0.1%) in the backward direction around zero detuning. Likewise, at the negative phase of $\theta = -0.73\pi$ the transmission from cavity 1 to 2 is suppressed while the transmission from cavity 2 to 1 is

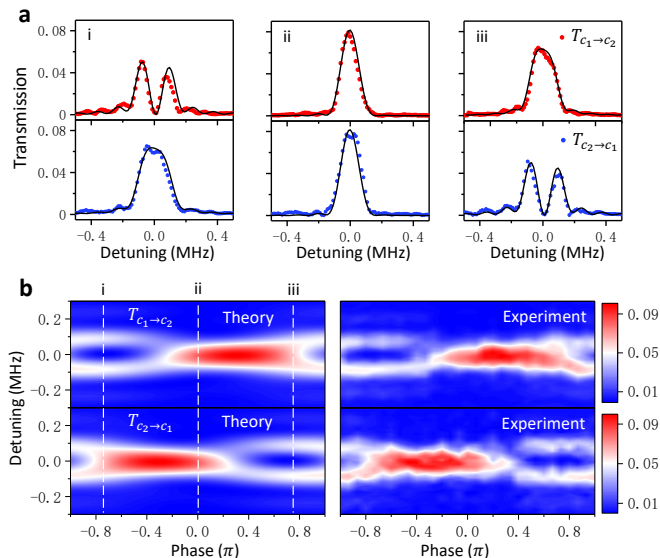


FIG. 3. **Non-reciprocal routing between the two optical modes.** **a.** Measured transmission spectra $T_{c_1 \rightarrow c_2}$ (red dots) and $T_{c_2 \rightarrow c_1}$ (blue dots) as a function of probe detuning, shown in both directions for control phases $\theta = 0.73\pi$, 0 , -0.73π . The solid lines show the results of theoretical calculations. Isolation of more than 15 dB in both directions is demonstrated with a bandwidth of 17.7 kHz, as well as reciprocal behaviour with $\theta = 0$. **b.** Theoretical and experimental transmission spectra $T_{c_1 \rightarrow c_2}$ and $T_{c_2 \rightarrow c_1}$ as a function of the control phase and probe detuning. Dashed lines correspond to the three measured phases as shown in **a**.

high. The peaks and dips with the linewidth of around $\sqrt{\gamma_1 \gamma_2}$ observed in Fig. 2a, highlight the two-path interference mediated by two mechanical modes. Isolation of more than 15 dB in both directions is demonstrated with a bandwidth of 17.7 kHz. Around $\theta = 0$, the frequency conversion is reciprocal and bidirectional. Figure 3b shows the transmission spectra as a function of probe detuning for the whole range of phases θ , where isolation of more than 15 dB is demonstrated in both directions. Here, we neglect the mode coupling between clockwise (CW) and counter-clockwise (CCW) whispering-gallery modes because of the weak backscattering. Actually, the traveling wave cavity supports a pair of degenerate optical modes. The CW modes c_1 and c_2 can be coupled with the CCW modes due to the strong optical backscattering or nanoparticles [48]. Therefore, the model can be built including two paired optical modes. Finally, the non-reciprocal routing of bosonic excitations between the optical mode c_1 and the mechanical mode m_1 is demonstrated. The details of which are discussed in Supplementary Material. Due to the symmetry, the phase-controlled non-reciprocal routing between arbitrary two bosonic modes with ultra-high frequency difference can be implemented.

The described four-mode plaquette can achieve flexible expansion, for example by parametrically coupling

a third mechanical mode m_3 to the optical modes, as shown in Fig. 4a. This five-mode plaquette is established in another silica microsphere with $\omega_{m_1}/2\pi = 75.3$ MHz, $\omega_{m_2}/2\pi = 76.4$ MHz and $\omega_{m_3}/2\pi = 112.7$ MHz (see Supplementary Material for more details). Similar to the four-mode case, we use six control fields with frequencies slightly detuned from the lower motional sidebands of the resonances to form the closed-loop. The powers of the control fields are $(P_{11}, P_{12}, P_{13}, P_{21}, P_{22}, P_{23}) = (4.8, 1.6, 4.2, 3.4, 1.6, 1.7)$ mW corresponding to the cooperativities $(C_{11}, C_{12}, C_{13}, C_{21}, C_{22}, C_{23}) = (1.6, 1.3, 1.3, 1.1, 0.86, 0.76)$. For an experimental demonstration of the phase-controlled phononic circulator, we measure the isolation $I_{ij} = 10 \log(T_{m_i \rightarrow m_j} / T_{m_j \rightarrow m_i})$ ($i, j \in \{1, 2, 3\}$) versus the control phases, as shown in Fig. 4b. Unlike the four-mode case, where the non-reciprocal conversion is achieved by varying only one control phase, in the phononic circulator, at least two independent control phases (θ_{11} and θ_{12} in our experiment) need to be tuned to change the phase difference of the three pairs of interference paths. As both θ_{11} and θ_{12} dominantly affect the transportation between mode m_1 and mode m_2 , I_{12} has a significant change in the diagonal direction, while I_{23} (I_{31}) changes dominantly upon θ_{12} (θ_{11}) varying, which is in agreement with intuition and theory (see Supplementary Material for more details). Figure 4c plots the $I_{sum} = I_{12} + I_{23} + I_{31}$, where we see phononic circulation in the forward direction I_{sum} of up to 35 dB at $(\theta_{11}, \theta_{12}) = (-0.7, 0.1)\pi$ or in the backward direction $I_{sum} = -33.3$ dB at $(\theta_{11}, \theta_{12}) = (0.7, -0.1)\pi$. Via a simple change in the control fields, the direction of circulator is reversed, demonstrating the great flexibility of our device.

Beyond the five-mode model, our demonstration can be scaled to the two-dimensional hybrid network by exploiting more optical and mechanical modes in the same microcavity, while each link couples one optical mode and one mechanical mode. Indeed, the transmission of photons between CW and CCW optical modes can also achieve non-reciprocal conversion mediated by one mechanical mode [12]. Because of the demonstration of non-reciprocal transportation between any two nodes, we can control the propagation of the bosonic excitations along the designated route (Supplementary Fig. S6). The expansion of the network in a single microcavity provides a potential platform for studying topological photonics/phononics and quantum many-body physics, without the requirement of fabricating massive identical microstructures.

In conclusion, we have experimentally demonstrated the non-reciprocal routing of phonon-phonon, photon-photon, and photon-phonon simultaneously in a single microresonator. The non-reciprocal routing is controlled by adjusting the frequency and phase of the control field. Among them, the optical non-reciprocal frequency conversion can reach 6% efficiency and 15dB isolation, and

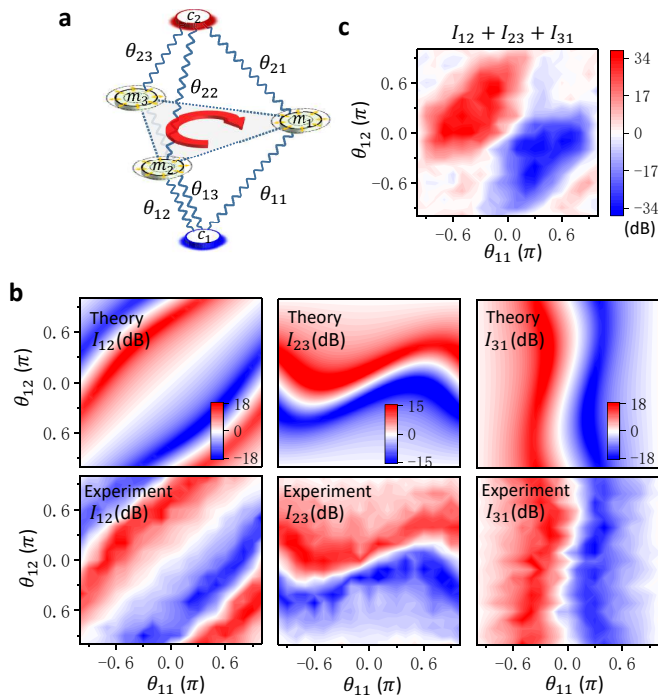


FIG. 4. **Phononic circulator.** **a.** Three mechanical modes m_1 , m_2 and m_3 and two optical modes c_1 and c_2 are used to establish a five-mode network, creating a circulatory conversion between the three mechanical modes, as indicated by the red arrow. **b.** The measured isolation $I_{ij} = 10 \log(T_{m_i \rightarrow m_j} / T_{m_j \rightarrow m_i})$ ($i, j \in \{1, 2, 3\}$) and theoretical model as a function of control phases θ_{11} and θ_{12} . **c.** The isolation $I_{12} + I_{23} + I_{31}$, indicating the circulator direction can be changed by control phases.

more than 15dB isolation for the phonon non-reciprocal conversion and circulation. These results can be applied to information processing and thermal management, and also lay a foundation for the directional routing of signals in a hybrid network.

Acknowledgments

The work was supported by the National Key R&D Program of China (Grant No.2016YFA0301303), the National Natural Science Foundation of China (Grant Nos. 61805229, 11874342, 11934012, and 92050109), USTC Research Funds of the Double First-Class Initiative (YD2470002002), the China Postdoctoral Science Foundation (Grant No. 2019M652181) and the Fundamental Research Funds for the Central Universities. This work was partially carried out at the USTC Center for Micro and Nanoscale Research and Fabrication.

Author contributions

Z.S. C.-L.Z. and C.-H. D. conceived and designed the experiment. Z.S., Y.C. and C.H.D. prepared the samples, built the experimental setup and carried out experiment measurements. Y.-L.Z. Y.-F. X. and C.-L.Z. provided

theoretical support and analysed the data. Z.S., C.-H.D. and C.-L.Z. wrote the manuscript with inputs from all authors. C.-H.D, and G.-C.G. supervised the project. All authors contributed extensively to the work presented in this paper.

Additional information

Supplementary information is available in the online version of the paper. Reprints and permissions information is available online at. Correspondence and requests for materials should be addressed to C.-H.D. (chunhua@ustc.edu.cn).

Competing financial interests

The authors declare no competing interests.

* These authors contributed equally to this work.

† chunhua@ustc.edu.cn

- [1] Z. Yu and S. Fan, “Complete optical isolation created by indirect interband photonic transitions,” *Nature photonics* **3**, 91 (2009).
- [2] Y. Shoji and T. Mizumoto, “Magneto-optical non-reciprocal devices in silicon photonics,” *Science and technology of advanced materials* **15**, 014602 (2014).
- [3] D. L. Sounas and A. Alù, “Non-reciprocal photonics based on time modulation,” *Nature Photonics* **11**, 774 (2017).
- [4] L. Bi, J. Hu, P. Jiang, D. H. Kim, G. F. Dionne, L. C. Kimerling, and C. Ross, “On-chip optical isolation in monolithically integrated non-reciprocal optical resonators,” *Nature Photonics* **5**, 758 (2011).
- [5] R. Fleury, D. L. Sounas, C. F. Sieck, M. R. Haberman, and A. Alù, “Sound isolation and giant linear nonreciprocity in a compact acoustic circulator,” *Science* **343**, 516 (2014).
- [6] S. Maayani, R. Dahan, Y. Kligerman, E. Moses, A. U. Hassan, H. Jing, F. Nori, D. N. Christodoulides, and T. Carmon, “Flying couplers above spinning resonators generate irreversible refraction,” *Nature* **558**, 569 (2018).
- [7] R. Huang, A. Miranowicz, J.-Q. Liao, F. Nori, and H. Jing, “Nonreciprocal photon blockade,” *Physical review letters* **121**, 153601 (2018).
- [8] W. Fu, Z. Shen, Y. Xu, C.-L. Zou, R. Cheng, X. Han, and H. X. Tang, “Phononic integrated circuitry and spin-orbit interaction of phonons,” *Nature communications* **10**, 1 (2019).
- [9] E. Verhagen and A. Alù, “Optomechanical nonreciprocity,” *Nature Physics* **13**, 922 (2017).
- [10] H. Xu, L. Jiang, A. Clerk, and J. Harris, “Nonreciprocal control and cooling of phonon modes in an optomechanical system,” *Nature* **568**, 65 (2019).
- [11] J. P. Mathew, J. Del Pino, and E. Verhagen, “Synthetic gauge fields for phonon transport in a nano-optomechanical system,” *Nature nanotechnology* **15**, 198 (2020).
- [12] Y. Chen, Y.-L. Zhang, Z. Shen, C.-L. Zou, G.-C. Guo, and C.-H. Dong, “Synthetic gauge field in a single optomechanical resonator,” *Physical review letters* **126**,

- 123603 (2021).
- [13] M. Merklein, B. Stiller, K. Vu, P. Ma, S. J. Madden, and B. J. Eggleton, "On-chip broadband nonreciprocal light storage," *Nanophotonics* **1** (2020).
- [14] H. Lira, Z. Yu, S. Fan, and M. Lipson, "Electrically driven nonreciprocity induced by interband photonic transition on a silicon chip," *Physical review letters* **109**, 033901 (2012).
- [15] L. D. Tzauang, K. Fang, P. Nussenzevig, S. Fan, and M. Lipson, "Non-reciprocal phase shift induced by an effective magnetic flux for light," *Nature photonics* **8**, 701 (2014).
- [16] C.-H. Dong, Z. Shen, C.-L. Zou, Y.-L. Zhang, W. Fu, and G.-C. Guo, "Brillouin-scattering-induced transparency and non-reciprocal light storage," *Nature communications* **6**, 6193 (2015).
- [17] J. Kim, M. C. Kuzyk, K. Han, H. Wang, and G. Bahl, "Non-reciprocal brillouin scattering induced transparency," *Nature Physics* **11**, 275 (2015).
- [18] T. Devaux, V. Tournat, O. Richoux, and V. Pagneux, "Asymmetric acoustic propagation of wave packets via the self-demodulation effect," *Physical review letters* **115**, 234301 (2015).
- [19] D. B. Sohn, S. Kim, and G. Bahl, "Time-reversal symmetry breaking with acoustic pumping of nanophotonic circuits," *Nature Photonics* **12**, 91 (2018).
- [20] E. A. Kittlaus, W. M. Jones, P. T. Rakich, N. T. Otterstrom, R. E. Muller, and M. Rais-Zadeh, "Electrically driven acousto-optics and broadband non-reciprocity in silicon photonics," *Nature Photonics* **15**, 43 (2021).
- [21] M. Scheucher, A. Hilico, E. Will, J. Volz, and A. Rauschenbeutel, "Quantum optical circulator controlled by a single chirally coupled atom," *Science* **354**, 1577 (2016).
- [22] S. Zhang, Y. Hu, G. Lin, Y. Niu, K. Xia, J. Gong, and S. Gong, "Thermal-motion-induced non-reciprocal quantum optical system," *Nature Photonics* **12**, 744 (2018).
- [23] X.-X. Hu, Z.-B. Wang, P. Zhang, G.-J. Chen, Y.-L. Zhang, G. Li, X.-B. Zou, T. Zhang, H. X. Tang, C.-H. Dong, *et al.*, "Noiseless photonic non-reciprocity via optically-induced magnetization," *Nature communications* **12**, 2389 (2021).
- [24] M. F. Lewis and E. Patterson, "Acoustic-surface-wave isolator," *Applied Physics Letters* **20**, 276 (1972).
- [25] R. Sasaki, Y. Nii, Y. Iguchi, and Y. Onose, "Nonreciprocal propagation of surface acoustic wave in ni/linbo₃," *Phys. Rev. B* **95**, 020407 (2017).
- [26] T. J. Kippenberg and K. J. Vahala, "Cavity optomechanics," *Optics express* **15**, 17172 (2007).
- [27] M. Aspelmeyer, T. J. Kippenberg, and F. Marquardt, "Cavity optomechanics," *Reviews of Modern Physics* **86**, 1391 (2014).
- [28] M. Hafezi and P. Rabl, "Optomechanically induced non-reciprocity in microring resonators," *Optics express* **20**, 7672 (2012).
- [29] Y. Li, Y. Huang, X. Zhang, and L. Tian, "Optical directional amplification in a three-mode optomechanical system," *Optics express* **25**, 18907 (2017).
- [30] Z. Shen, Y.-L. Zhang, Y. Chen, C.-L. Zou, Y.-F. Xiao, X.-B. Zou, F.-W. Sun, G.-C. Guo, and C.-H. Dong, "Experimental realization of optomechanically induced non-reciprocity," *Nature Photonics* **10**, 657 (2016).
- [31] F. Ruesink, M.-A. Miri, A. Alu, and E. Verhagen, "Nonreciprocity and magnetic-free isolation based on optomechanical interactions," *Nature communications* **7**, 1 (2016).
- [32] Z. Shen, Y.-L. Zhang, Y. Chen, F.-W. Sun, X.-B. Zou, G.-C. Guo, C.-L. Zou, and C.-H. Dong, "Reconfigurable optomechanical circulator and directional amplifier," *Nature communications* **9**, 1797 (2018).
- [33] E. A. Kittlaus, N. T. Otterstrom, P. Kharel, S. Gertler, and P. T. Rakich, "Non-reciprocal interband brillouin modulation," *Nature Photonics* **12**, 613 (2018).
- [34] K. Fang, J. Luo, A. Metelmann, M. H. Matheny, F. Marquardt, A. A. Clerk, and O. Painter, "Generalized non-reciprocity in an optomechanical circuit via synthetic magnetism and reservoir engineering," *Nature Physics* **13**, 465 (2017).
- [35] F. Ruesink, J. P. Mathew, M.-A. Miri, A. Alù, and E. Verhagen, "Optical circulation in a multimode optomechanical resonator," *Nature communications* **9**, 1798 (2018).
- [36] A. Seif, W. DeGottardi, K. Esfarjani, and M. Hafezi, "Thermal management and non-reciprocal control of phonon flow via optomechanics," *Nature communications* **9**, 1 (2018).
- [37] G. A. Peterson, F. Lecocq, K. Cicak, R. W. Simmonds, J. Aumentado, and J. D. Teufel, "Demonstration of efficient nonreciprocity in a microwave optomechanical circuit," *Physical Review X* **7**, 031001 (2017).
- [38] S. Barzanjeh, M. Wulf, M. Peruzzo, M. Kalaei, P. Dieterle, O. Painter, and J. M. Fink, "Mechanical on-chip microwave circulator," *Nature communications* **8**, 1 (2017).
- [39] N. R. Bernier, L. D. Toth, A. Koottandavida, M. A. Ioannou, D. Malz, A. Nunnenkamp, A. Feofanov, and T. Kippenberg, "Nonreciprocal reconfigurable microwave optomechanical circuit," *Nature communications* **8**, 1 (2017).
- [40] A. Metelmann and A. A. Clerk, "Nonreciprocal quantum interactions and devices via autonomous feedforward," *Phys. Rev. A* **95**, 013837 (2017).
- [41] D. Malz, L. D. Tóth, N. R. Bernier, A. K. Feofanov, T. J. Kippenberg, and A. Nunnenkamp, "Quantum-limited directional amplifiers with optomechanics," *Physical review letters* **120**, 023601 (2018).
- [42] L. Mercier de Lépinay, C. F. Ockeloen-Korppi, D. Malz, and M. A. Sillanpää, "Nonreciprocal transport based on cavity floquet modes in optomechanics," *Phys. Rev. Lett.* **125**, 023603 (2020).
- [43] C. Dong, V. Fiore, M. C. Kuzyk, and H. Wang, "Optomechanical dark mode," *Science* **338**, 1609 (2012).
- [44] J. T. Hill, A. H. Safavi-Naeini, J. Chan, and O. Painter, "Coherent optical wavelength conversion via cavity optomechanics," *Nature communications* **3**, 1 (2012).
- [45] Y. Liu, M. Davanço, V. Aksyuk, and K. Srinivasan, "Electromagnetically induced transparency and wide-band wavelength conversion in silicon nitride microdisk optomechanical resonators," *Physical review letters* **110**, 223603 (2013).
- [46] V. Fiore, Y. Yang, M. C. Kuzyk, R. Barbour, L. Tian, and H. Wang, "Storing optical information as a mechanical excitation in a silica optomechanical resonator," *Phys. Rev. Lett.* **107**, 133601 (2011).
- [47] V. Fiore, C. Dong, M. C. Kuzyk, and H. Wang, "Optomechanical light storage in a silica microresonator," *Physical Review A* **87**, 023812 (2013).
- [48] J. Zhu, S. K. Ozdemir, Y.-F. Xiao, L. Li, L. He, D.-R.

Chen, and L. Yang, "On-chip single nanoparticle de-

tection and sizing by mode splitting in an ultrahigh-q microresonator," *Nature photonics* **4**, 46 (2010).